LAWRENCE
LIVERMORE
NATIONAL
LABORATORY

LLNL-TR-713677

Thermal aging of traditional and additively manufactured foams: analysis by time-temperature-superposition, constitutive, and finite-element models

A. Maiti, T. H. Weisgraber, W. Small, J. P. Lewicki, E. B. Duoss, C. M. Spadaccini, M. A. Pearson, S. C. Chinn, T. S. Wilson, R. S. Maxwell

December 8, 2016

Disclaimer

This work performed under the auspices of the U.S. Department of Energy by Lawrence Livermore National Laboratory under Contract DE-AC52-07NA27344.

Thermal aging of traditional and additively manufactured foams: analysis by time-temperature-superposition, constitutive, and finite-element models

A. Maiti, T. H. Weisgraber, W. Small, J. P. Lewicki, E. B. Duoss, C. M. Spadaccini, M. A. Pearson, S. C. Chinn, T. S. Wilson, R. S. Maxwell

Abstract:

Cellular solids or foams are a very important class of materials with diverse applications ranging from thermal insulation and shock absorbing support cushions, to light-weight structural and floatation components, and constitute crucial components in a large number of industries including automotive, aerospace, electronics, marine, biomedical, packaging, and defense. In many of these applications the foam material is subjected to long periods of continuous stress, which can, over time, lead to a permanent change in structure and a degradation in performance. In this report we summarize our modeling efforts to date on polysiloxane foam materials that form an important component in our systems. Aging of the materials was characterized by two measured quantities, i.e., compression set and load retention. Results of accelerated aging experiments were analyzed by an automated time-temperature-superposition (TTS) approach, which creates a master curve that can be used for long-term predictions (over decades) under ambient conditions. When comparing such master curves for traditional (stochastic) foams with those for recently 3D-printed (i.e., additively manufactured, or AM) foams, it became clear that AM foams have superior aging behavior. To gain deeper understanding, we imaged the microstructure of both foams using X-ray computed tomography, and performed finite-element analysis of the mechanical response within these microstructures. This indicates a wider stress variation in the stochastic foam with points of more extreme local stress as compared to the 3D printed material.

Compression Set and Load Retention

Two quantities that were used to characterize the aging of foams were compression set and load retention. Compression set ($S(t)$) is defined as the ratio of the decrease in sample thickness (after periodic removal of stress) at time t to the original engineering compression at time zero. In terms of the original specimen thickness h_0 (before aging), the compressed thickness h_c, and the uncompressed thickness (at time t) h_t, it is given by:

$$S(t) = \frac{h_0 - h_t}{h_0 - h_c} = \frac{h_0 - h_t}{\varepsilon h_0} \quad , \qquad (1)$$

where ε is the engineering compressive strain (see Fig. A1 in Appendix I). Load retention ($R(t)$) is defined by the ratio of the load at time t (F_t) measured while the specimen is under the long-term compressive strain (during aging)

to the corresponding load at time zero (F_0) at the beginning of the aging study, i.e.,

$$R(t) = {}^{F_t}/_{F_0}. \qquad (2)$$

The above definitions of $S(t)$ and $R(t)$ make them relatively insensitive to the level of long-term strain employed, and thus make them comparable across all our experiments where the strain level varies between 25-35%. Note that both definitions above are properly normalized, i.e., compression set $S(t)$ starts out with a value of 0% and increases toward a theoretical maximum value of 100%, which indicates complete loss of functionality. It is exactly the opposite for load retention, which starts out at an initial value of 100% and decreases monotonically toward a theoretical minimum of 0%, which represents complete lack of mechanical response. Conditions and parameters for the aging studies on different foams are summarized in Table A1 in Appendix I. It is to be noted that compression set and load retention are not completely uncorrelated quantities – higher compression set is usually associated with lower load retention, given that the former implies less amount of load needed to get back to the original strain level. Additionally, load retention also includes effects of evolution in mechanical modulus as a function of time. Thus, together $S(t)$ and $R(t)$ provide a good description of the mechanical response state of the material and constitute good indicators of performance as a function of time. As far as measurement errors in our experiments, we estimate errors in thickness measurements to be less than 0.2% and errors in force measurements to be within 3%. Thus, all our compression set and load retention results reported below are accurate to within a few percent.

Figure 1 (top left) displays the compression set of the stochastic foam M9763 measured over a period of two years at four different temperatures: room temperature (i.e. ambient conditions), 35, 50, and 70°C. In order to predict the long-time evolution of the compression set under ambient conditions, we performed a procedure called time-temperature superposition (TTS) [1, 2], in which each isotherm is rigidly shifted along the logarithmic time axis so as to generate a single "master" curve. In the literature one often encounters examples, especially on thermo-rheological response of polymers and composites, where such curves are manually shifted "by eye". Although such manual shifting is acceptable for properties that can be accurately measured with little noise, in many cases such a procedure often can be subjective [3, 4] and may lead to large errors in long-term prediction. Given that the present work involves comparison of measurements on two different materials conducted over vastly different time-durations, a more accurate and objective method was necessary. To this end, we employed a recently developed geometry-based algorithm of TTS shifting [5, 6], in which the optimum master curve is defined as the one corresponding to the minimum vertical arc-length, given by the formula:

$$d = \left\{\sum_{k=1}^{N-1}(y_{k+1} - y_k)^2\right\}^{1/2}, \qquad (3)$$

where $\{y_k | \, k = 1, 2, \ldots, N\}$ represent all observations at all different temperatures that have been arranged in the ascending order of shifted times. A schematic representation of the minimization procedure is provided in Fig. A3 in Appendix II. More details are described in Appendix II and elsewhere [6]. Figure 1(top right) shows the optimized master curve for the compression set data of Fig. 1(top left) obtained by following the above TTS procedure. For the

purpose of comparison between different foams, we also provide a smooth prediction curve defined by the three-parameter function:

$$f_S(t) = 1 - \left\{1 + \frac{1}{n}\left(\frac{t}{\tau}\right)^m\right\}^{-n} \quad , \qquad (4)$$

where the parameters m, n, and τ are obtained by minimizing the mean-square vertical deviation of the data points in the master curve from the prediction curve, and in the plot we multiply the function $f_S(t)$ by 100 and express as percent (%). Fig. 1 (bottom left) displays the measured load retention of a M9763 foam with data taken over a period of 8.5 years (measurements performed at NSC (formerly KCP)) at room temperature, 50, and 70°C, while Fig. 1 (bottom right) shows the master curve formed by the TTS-shifted data along with a smooth prediction master curve defined by the function:

$$f_R(t) = \left\{1 + \frac{1}{n}\left(\frac{t}{\tau}\right)^m\right\}^{-n}. \qquad (5)$$

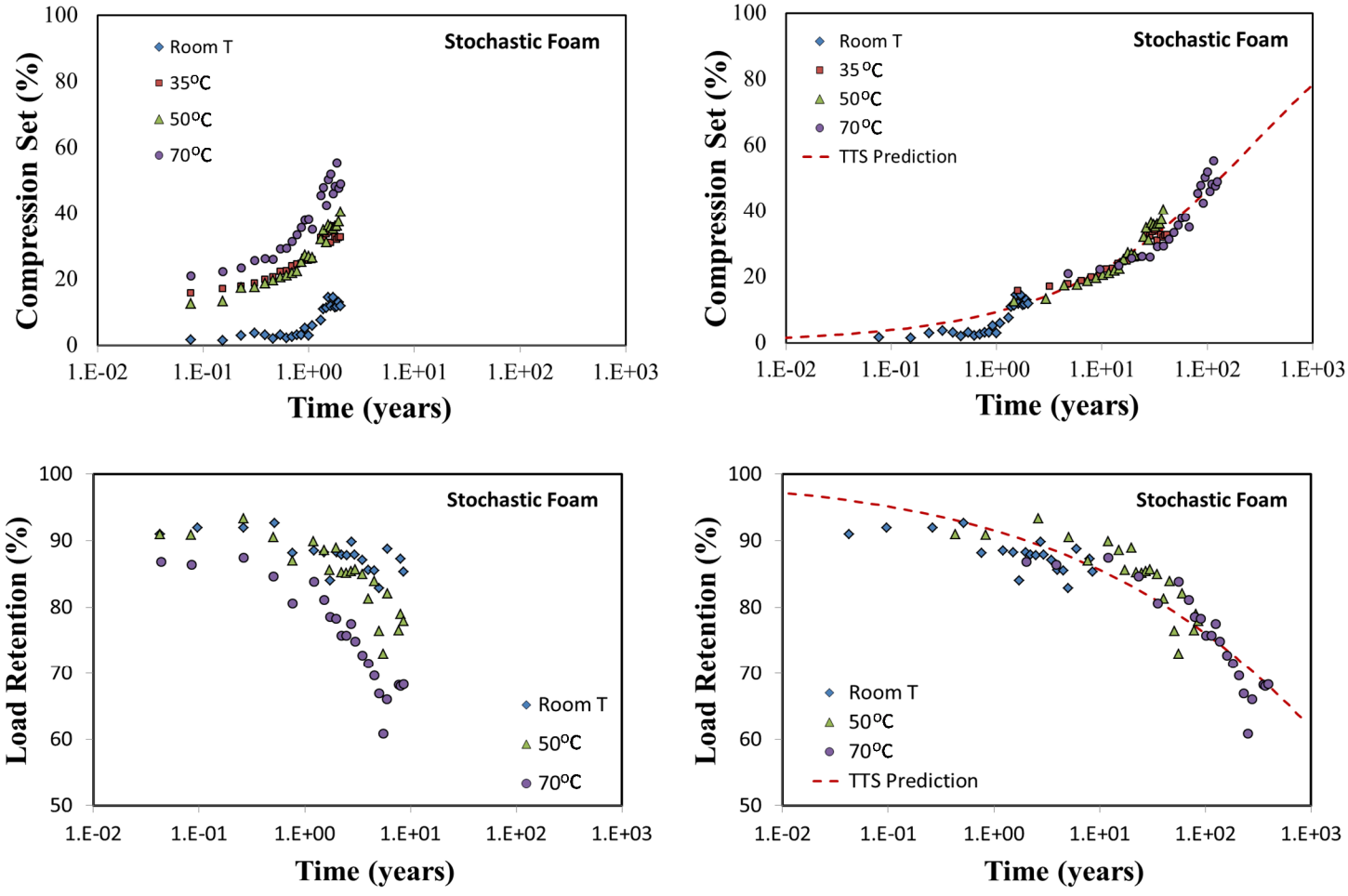

Figure 1. Compression set (top left) and load retention (bottom left) of legacy foam M9763. The left figures are actual measurements taken as a function of time over a period of 2 years for compression set and 8.5 years for load retention. The right figures are obtained by TTS-shifting the isotherms along the log-time axis to obtain a single master-curve with the minimum arc-length [6]. The dashed curves (TTS Prediction) are smooth fits to the master curve, and used for prediction purposes.

Data collection over a much longer time for load retention was necessitated by the requirement of property prediction over a period of several decades, in line with extended service times in many applications involving structural support foams.

Material: M97*, S5370, S5455, AM FCT

Similar compression set and load retention measurements were performed on a number of other relevant foam materials including, M97*, S5370, S5455, and more recently on additively manufactured (AM) foams of the face-centered tetragonal (FCT) structure. For the S5370 and S5455 foams only the compression set data were available. All the aging data were analyzed with the automated TTS procedure as described above for M9763. Below in Fig. 2 we compare the 100-year predictions from the TTS master curves of all these foams.

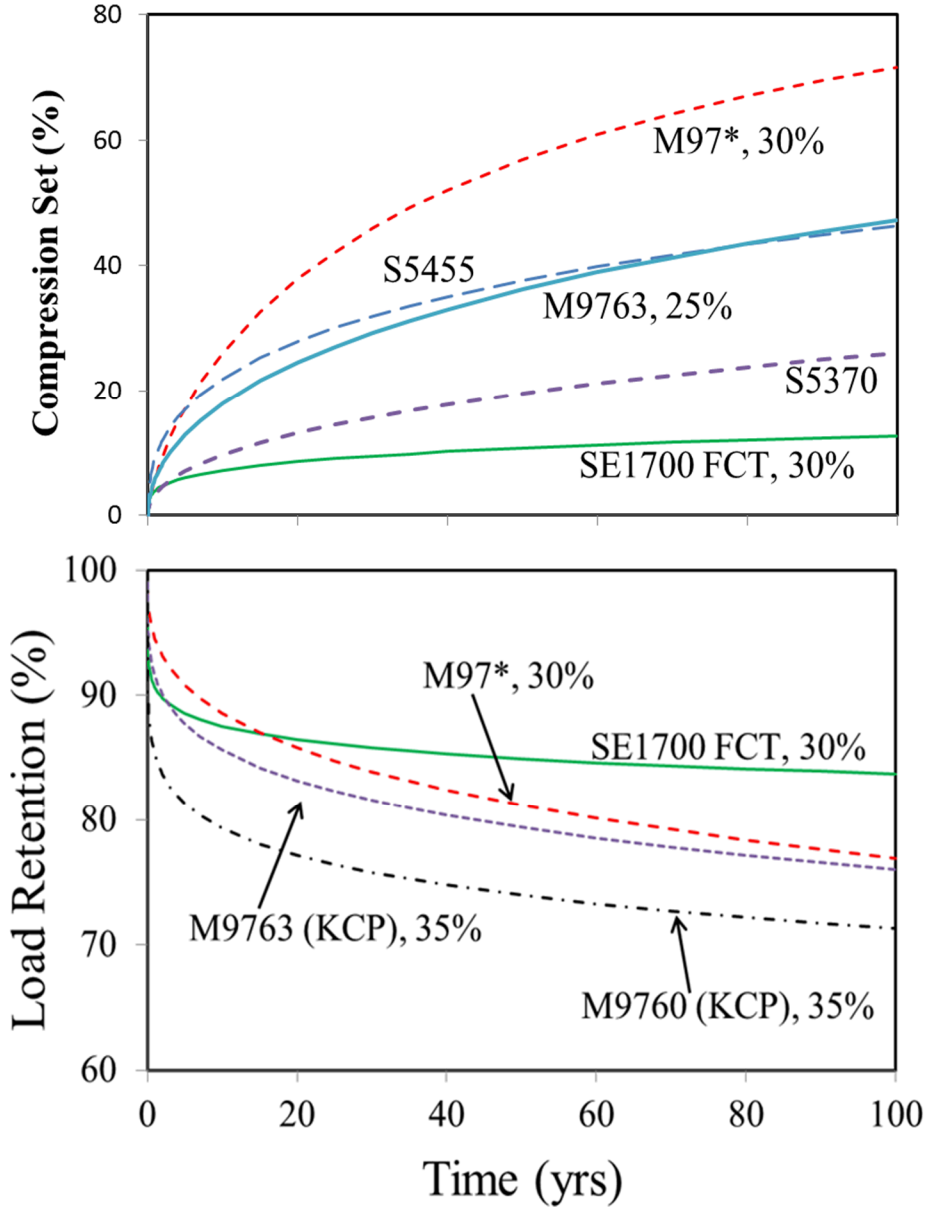

Figure 2. TTS-predicted compression set (top figure) and load retention (bottom figure) for a number of legacy (stochastic) foams and AM foam (SE1700 FCT) under ambient conditions over a period of 100 years.

X-ray CT and Finite Element Modeling (M9763):

Background

Polymer foams serve as critical components in the stockpile and our goals are to understand the material behavior and quantify the uncertainty in the mechanical properties of these components over the lifetimes of the relevant systems. When compressed, foams exhibit a stress response determined by both the intrinsic properties of the elastomer and the complex open-cell microstructure. At small strains, the elastic deformation of the structure produces a nearly linear regime, followed by a plateau region indicative of the buckling of cell walls. Further compression eliminates most of the void structure and the stress dramatically increases as the material densifies.

Initial efforts to elucidate the foam structure-property relationships focused on simple geometric unit cells using analytical techniques [7]. More complex geometries assembled from arrays of unit cells are amenable to finite element analysis, though for a given material it is difficult to construct a representative microstructure. The development of X-ray computed tomography (CT) enabled non-destructive detailed characterization of foams and the resulting voxel data can be processed to generate a surface representation for a finite element code [8].

Here, we report a concerted application of X-ray CT and finite element modeling to samples of M9763 foam from a yearlong aging study. Our goals are to enhance our understanding of the complex morphology and mechanical property relationship and to develop the most representative translation of the voxel data into a finite element model. With finite element analysis, we can decouple the aging-related alterations to the porous structure from chemical changes in the material microstructure, both of which contribute to changes in the material response. By exploiting analytical aging models and experimental data we can explore the relative contributions of the aged bulk material and porous architectures.

X-ray CT

Four samples of M9763 were placed between shims within a compression rig with an applied strain of 25% for a 12-month aging study within a room temperature desiccated environment. Each sample was a 10 mm diameter disk with a thickness of 1 mm. At the end of each month, the loaded samples were exposed to an x-ray source for imaging, followed by the removal of the applied strain and a 24-hour relaxation period. The unloaded samples were again imaged to study changes in microstructure and measure the amount of compression set before returning them to a state of 25% compression for another month. Fig. 3 shows images of the reconstructed loaded and unloaded data sliced at the mid-plane to reveal the internal foam structure.

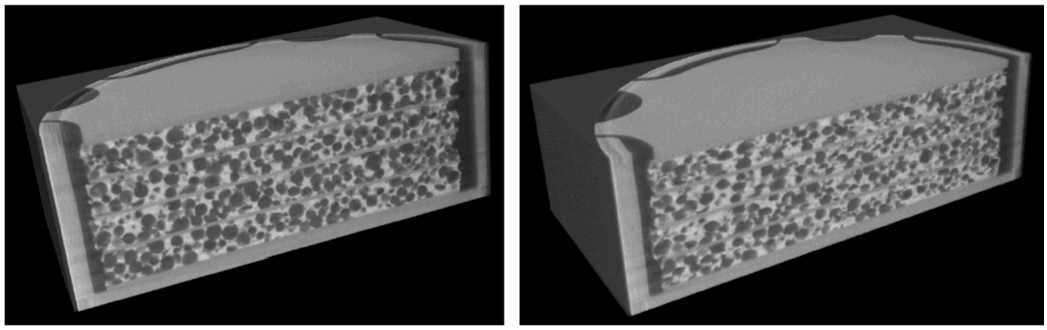

Figure 3. CT volume renderings of the M9763 samples within the compression rig in the unloaded and loaded states.

Finite element modeling

The raw CT data consisted of a series of images representing consecutive slices of the compression rig and its contents. These images were concatenated to a 3D rendering by the Simpleware visualization software, which also smoothed and segmented the data to extract a voxel-based representation of the foam. With this voxel template, Simpleware converted the data into a tetrahedral volume mesh, which was then translated into finite elements by a custom script designed specifically for this work.

The finite element simulations were performed with Paradyn, a parallel version of the Dyna3D explicit solver, developed at Lawrence Livermore National Laboratory [9]. The domains consisted of an $80 \times 80 \times 1$ mm volume extracted from one of the M9763 disks. Two thin plates of a stiff material bounded the upper and lower regions of the domain and provided loading and additional constraints for the simulations; a linear displacement was applied to the upper plate while the lower one remained fixed. The mesh for the foam contained approximately 7 million elements with an average size of 24 microns. The progression from voxel data, to a meshed finite element model is presented in Fig. 4.

To develop a materials model for the simulations, a series of uniaxial cyclic compression tests were conducted of the pure elastomer M9787 from which the foam was produced. Cylindrical specimens with a diameter of 8 mm and a 1.9 mm thickness were compressed in an Instron 5967 at a rate of 0.2 mm/min. A lubricant was applied to the platens to minimize friction. Because of some initial compression set caused by the Mullins effect, the third loading cycle was selected to approximate by the two-parameter Mooney-Rivlin constitutive model [10],

$$\sigma_{eng} = \left(2C_1 + \frac{2C_2}{\lambda}\right)\left(\lambda - \frac{1}{\lambda^2}\right), \qquad (6)$$

where $\lambda = 1 + \varepsilon_{eng}$ and the subscript *eng* denotes engineering stress and strain. The model provided an excellent fit to the experimental data (cycle 3 in Fig. 5) and was incorporated into the finite element simulations.

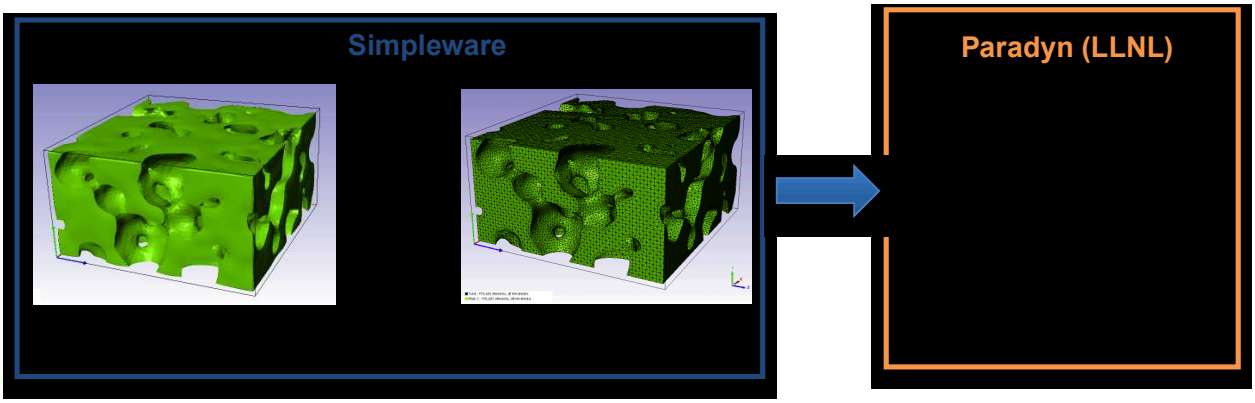

Figure 4. Depiction of the workflow from the CT data to a finite element mesh.

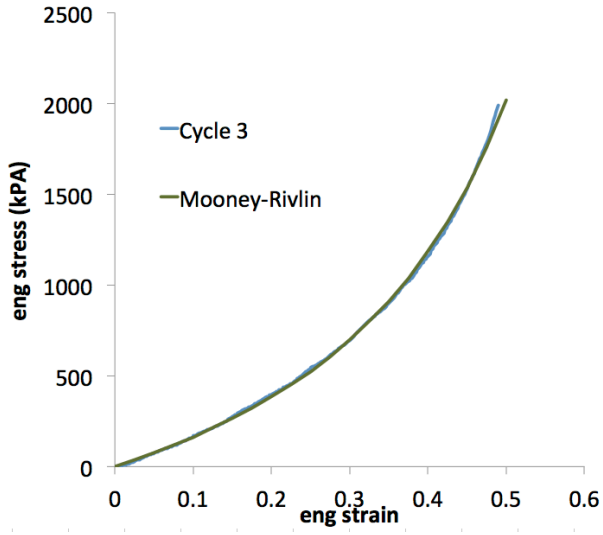

Figure 5. Comparison of compression data of M9787 with the Mooney-Rivlin model for the finite element simulations.

The applied loading at the top plate was implemented as both a constant velocity and linear displacement. Simulations with the displacement condition ran significantly faster by more than a factor of two. Measurement of the reactive force on the lower fixed plate provided the stress response data.

Fig. 6 shows a representative foam domain at 0% and 40% compression during the finite element simulation. With dynamic simulations we can achieve compressions that exceed 50% before elements deformation exceeds reasonable bounds due to the large contact forces.

The mechanical response from compression is plotted in Fig. 7 for the lower (represented by the blue curves) and upper (represented by the green curves) foam sample in the stack. The solid lines denote the pristine samples

and the dashed curves show the response of the aged materials after nine months of desiccation. Some sample variation is evident (difference between the green and blue solid curves) at compressive strains larger than 15%. However this variability is small when compared to the change in the response after nine months. Both upper and lower foams exhibited softening behavior due to changes in the porous architecture. (At the time of this publication the simulation of the aged upper foam had only run to 6% compression.) Analysis of the CT images revealed the surface to volume ratio of both foams increased after nine months from approximately 11 mm^{-1} to 13 mm^{-1}. Our hypothesis is the desiccated foam becomes more brittle and the repeated unloading and loading provides a damage mechanism whereby new voids form, allowing more air pockets which would reduce the elastic modulus. The formation of more void space is consistent with the increase in surface to volume ratio. A more thorough analysis of the pore size distribution is required to confirm this change in the foam structure.

Figure 6. Finite element modeling of a CT foam sample under uniaxial compression.

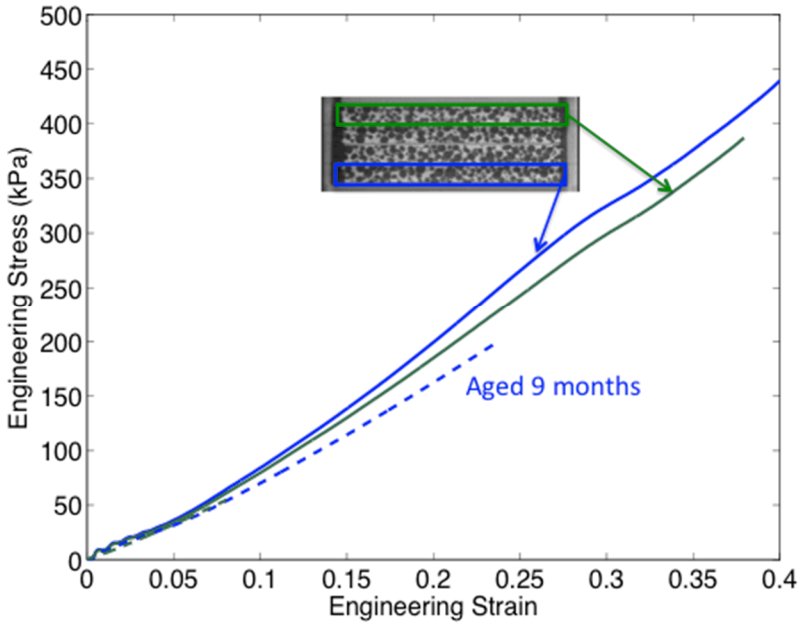

Figure 7. Foam stress response under uniaxial compression compared with the Mooney-Rivlin constitutive model for the bulk elastomer.

In summary, we have developed an approach to translate foam CT data into a finite element model in order to investigate the mechanical properties of foams compressed under various aging conditions. With this approach we can decouple the effects of chemical modification of the polymer network and the macroscopic changes in the porous structure. We continue to explore the relationship between morphology and mechanical properties while also quantifying the changes in pore size distribution. Age aware models of the elastomer will also be incorporated in the finite element simulations to help validate constitutive foam models and identify high stress concentration regions.

Internal stress distribution (*comparison between M9763 and AM FCT foams*):

The geometries and meshes of the M9763 and AM FCT foams were generated using two different approaches. For the stochastic M9763 foam, a solid region with a square cross section was first extracted from the X-ray CT data using the cropping, segmentation, and smoothing capabilities in ScanIP from Simpleware [11]. A tetrahedral conformal mesh was then produced from the voxel data based on a variant of the marching cube method. The resulting mesh was verified to have the same known porosity of the M9763 foam. To match this porosity for the FCT architectures, we created a domain consisting of 8 layers of D=250 μm diameter filaments with a pitch of 605 μm and an interlayer center-to-center spacing of 0.85D. An automated scripting tool assembled the geometry and tetrahedral mesh. Two thin stiff plates bounded the vertical extents of the two foams and provided a means of compressing the upper surface through a linear displacement while constraining the lower surface. The materials model for both structures was derived from experimental compression measurements of a cylindrical specimen of the bulk rubber (SE 1700) used to synthesize the AM foam. The stress response curve was fit to a Mooney-Rivlin constitutive equation [10] using a global optimization method to determine the coefficients. Quasi-static finite element simulations using the NIKE implicit code [12, 13] produced the overall mechanical response and local stress contours within the domains.

Figure 8 shows the von Mises stress magnitude [14] at representative lateral cross-sections of both architectures at 15% strain. The FCT plane intersects the overlap region between layers so filaments in both directions are visible. The direct ink write foam clearly exhibits uniform pore size and spacing whereas the M9763 foam contains a distribution of pore sizes with several in close contact. This clustering and overlapping of pores produces thin walls and highly concave topologies resulting in local stress concentrations indicated by the yellow and red regions in the figure. These points of high stresses are possibly the driving force behind irreversible damage to the foam microstructure, including strut fracture and pore collapse. On the other hand, consistent with its uniform architecture, the AM FCT foam exhibits highly repeatable and more uniform stress contours in both filament orientations with magnitudes less than a factor of two below the maximum stress in the M9763 [15].

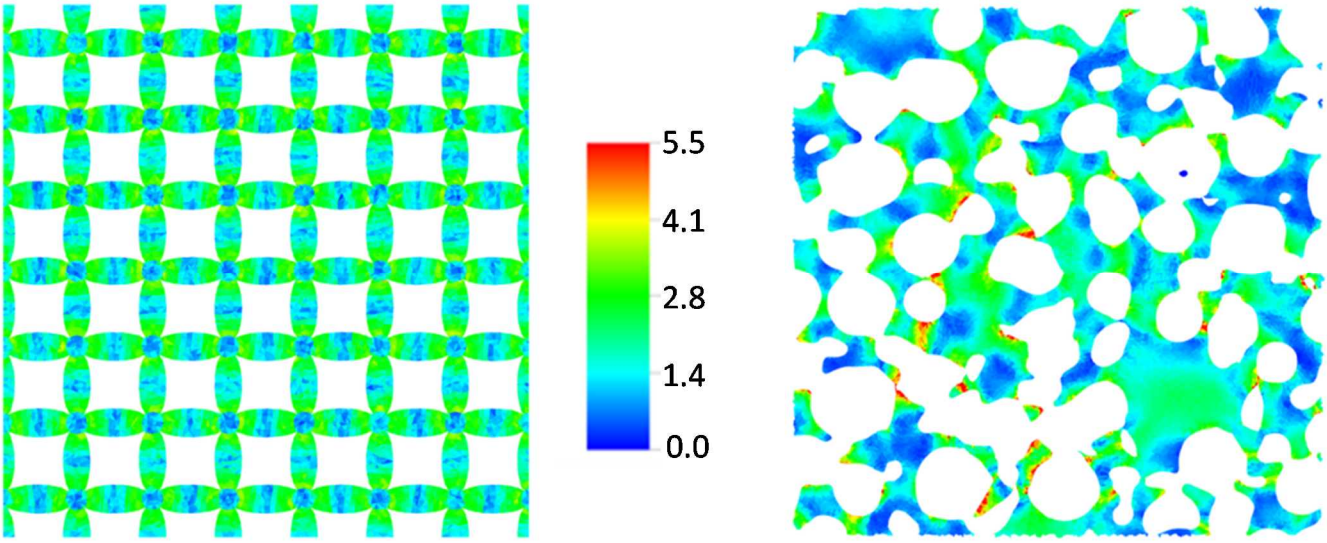

Figure 8. Stress distribution in a typical slice of: (left) AM FCT foam; and (right) stochastic foam M9763, both under 15% compressive strain. The presence of many high stress points is clearly evident in the stochastic foam. The presence of these high-stress points over an extended period of time is likely responsible for higher compression set and lower load retention in the stochastic foam as compared to the AM FCT foam. The stress scale bar is in units of 10^5 Pa.

Hyperelastic Foam Model (M9763)

Our past efforts on developing aging models for foams centered on predicting long-time evolution of compression set and load retention. However, to integrate such knowledge into system performance, it is necessary to tie in such quantities with mechanical stress-strain response models that ultimately feed into relevant physics-based simulations. To this end, an engineering group in DTED is actively developing hyperelastic foam models. Over the last few months we have been collaborating with this group in developing appropriate model parameters to describe experimental stress-strain data on M9763. Below is a summary of progress so far.

Ogden model:

Strain Energy Function (for general strain) [14, 16]:

$$W(F) = \sum_{i=1}^{N} \frac{2\mu_i}{{\alpha_i}^2}\left[({\lambda_1}^{\alpha_i} + {\lambda_2}^{\alpha_i} + {\lambda_3}^{\alpha_i} - 3) + \frac{1}{\beta_i}(J^{-\alpha_i\beta_i} - 1)\right] \qquad (7)$$

where, $J = \lambda_1\lambda_2\lambda_3$, μ_i can be thought of as effective shear moduli, and β_i are related to Poisson's ratio (in particular β_i=0 when Poisson's ratio = 0)

Uniaxial response: (σ_1= engineering stress)

$$\sigma_1 = \frac{2}{\lambda_1}\sum_{i=1}^{N} \frac{\mu_i}{\alpha_i}\left({\lambda_1}^{\alpha_i} - J^{-\alpha_i\beta_i}\right) \qquad (8)$$

The above model (for $N = 2$) was fitted to the loading curve in the fourth cycle of the stress-strain response of a M9763 specimen that was undergoing a uniaxial compression under lateral confinement (Fig. 9). As can be seen, the experimental response is described quite well by the Ogden model up to compression very close to lock-up. However, for a more effective model we would like to incorporate extensions that can quantitatively describe the following effects:

1. There is some observed hysteresis in the experimental curve, i.e., the stress in the unloading part of the curve is slightly below that of the loading curve.

2. There is observed aging in the form of load retention and compression set

3. There is interest in exploring foam response under joint uniaxial compression and shear

We are looking at various approaches, including introducing time-dependence in some of the Ogden parameters, and adding viscoelastic effects in the response in the form of Prony series terms [17]. Another possibility is to adopt more complex Materials models [18], e.g., Model 67, as developed by Zywicz [19].

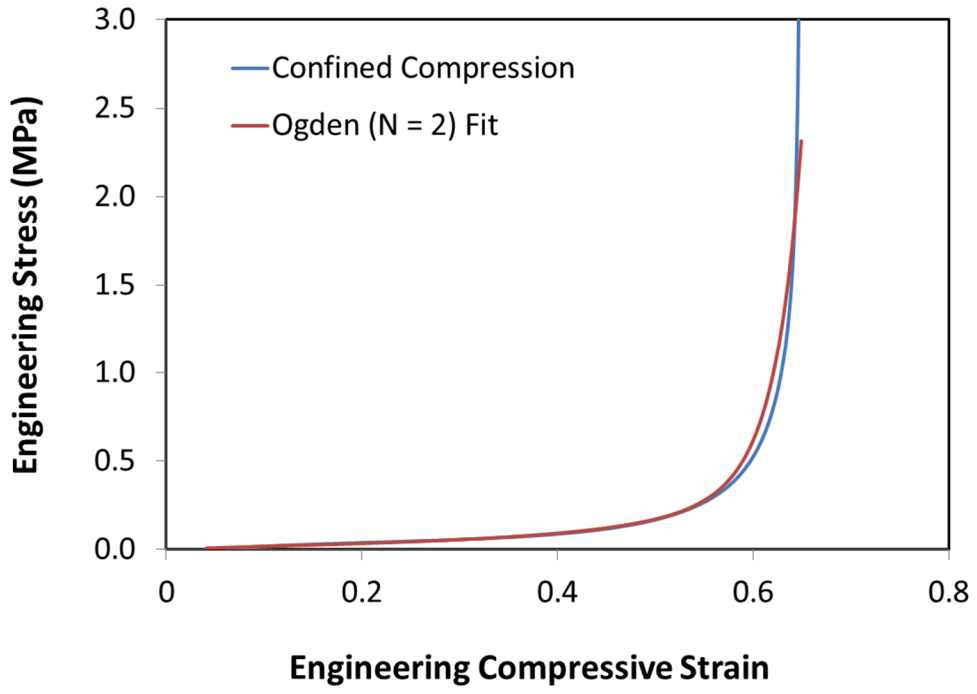

Figure 9. Fitting experimental uniaxial compression data for M9763 (i.e. compression under lateral confinement) with N = 2 Ogden model. Here we use the loading curve on the 4th cycle (specimen #2), and fitting is done for stress levels below 3 MPa.

APPENDIX I: Some Details of M9763/ M97*/ S5370 Aging Experiments

The M9763 material used in our study was an open-cell stochastic foam made by compounding a silica-reinforced PDMS resin with urea particles and curing at 121°C for 2 hours in a mold. The urea was leached out with water and the foam post-cured at 204°C for 18-24 hours, resulting in a stochastic foam 1.0 mm thick with ~ 63% porosity [20, 21].

Specimens were compressed in rigs comprised of two parallel steel plates bolted together with a given separation to achieve the desired compressive aging strain (25-35%) (see Fig. A1). Compressed specimens were aged at four different temperatures (room temperature, 35, 50, and 70°C). Uncompressed specimen thickness and load at the aging strain were periodically measured using a load tester. Heated specimens were allowed to cool to room temperature under compression prior to measurement. With the bolts removed, the compression rig containing the specimen was positioned in the tester and load applied until the compression rig itself was under load, as indicated by a sudden change in slope of the load deflection curve (Fig. A2). Some other experimental details are listed in Table A1 below.

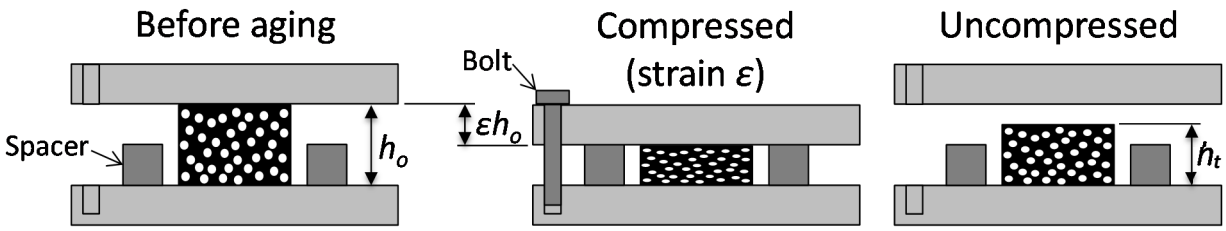

Figure A1. Schematic showing the various measured thicknesses used to define compression set: $S(t) = \frac{h_0 - h_t}{\varepsilon h_0}$.

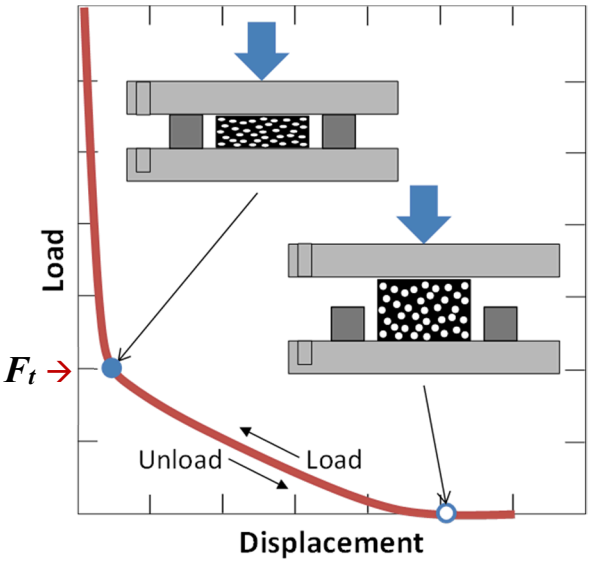

Figure A2. Schematic showing the measurement of force (load) under compression that is used to define load retention: $R(t) = F_t/F_0$; F_0 is the measured value of load at time zero, i.e. at the beginning of aging, while F_t is the measured value of load at time t. The force measurements are made at the bend in the load curve right before the sharp upward increase due to the compression of the rig blocks (closed dot). The difference between the displacement at the open dot (where the load begins to increase as the sample starts to undergo compression) and closed dot added to the spacer thickness gives the sample thickness used to calculate compression set.

Table A1: Conditions and parameters for accelerated aging studies on M9763 foam

	M9763 Foam Studies	
Values Measured	Compression set	Load retention
Study Duration	2 years	8.5 years
Aging Atmosphere	Dry nitrogen	Air (30-60% relative humidity)
Specimen Thickness	1.0 mm*	1.0 mm
Aging Strain	25%	35%
Aging Temperatures	Room T, 35, 50, 70°C	Room T, 50, 70°C

*Three specimens were stacked in each compression rig, separated by thin metal shims to prevent inter-digitation of the foam surfaces; all calculations accounted for the metal shim thickness.

APPENDIX II: Some Details of the automated TTS procedure

Background

Time-temperature-superposition (TTS) is a standard technique for generating a "master" prediction curve by rigidly shifting isotherms horizontally in the log-time axis. Previously, TTS shifting were performed "by eye". This process can be subjective, and can lead to significant error/ambiguity in long-term aging predictions. We have developed an objective approach to the shifting procedure through the optimization of vertical "arc-length" in the appropriate space (e.g., absolute difference in compression set or load retention of consecutive time-points in the TTS-shifted data).

Method

The method consists of the following steps:

- Suppose the property of interest y was measured at $N+1$ temperatures, i.e., $T_{ref} = T_0$, and N elevated temperatures $\{T_\alpha\}, \alpha = 1,2,\dots,N$. At each temperature T_α, let n_α measurements be taken at times $\{t_{i\alpha}\}, i = 1,2,\dots,n_\alpha$ with the measured values being $y_{i\alpha} = f(t_{i\alpha}, T_\alpha)$. The total number of measurements, therefore, is $n_{tot} = \sum_{\alpha=0}^{N} n_\alpha$.
- We arrange all the n_{tot} times $\{t_{i\alpha}\}$ in the ascending order. Let's call these sorted times $\{t_k\}, k = 1,2,\dots,n_{tot}$, and indicate the corresponding y-values as $\{y_k\}$.
- The total arc length d is defined in the form: $d = \left\{\sum_{k=1}^{n_{tot}-1} |\delta(y_{k+1}, y_k)|^n\right\}^{1/n}$
- $\delta(y_{k+1}, y_k)$ is a "distance function", which could be taken as linear or log
- We have mostly played with linear d and quadratic d $(n = 2)$.
- We apply time-shifts $\{a_\alpha\}$ to the elevated-T data: $t_{i\alpha} \to a_\alpha t_{i\alpha}$ $(\alpha = 1,2,\dots,N)$, i.e., all observation times at each elevated temperature $\{T_\alpha\}$ is horizontally shifted along the logarithmic time axis by an amount $\log(a_\alpha)$. The arc length d is then re-computed using the procedure outlined above.
- The optimized TTS shifts $\{a_\alpha^*\}$ correspond to the ones that minimize d.

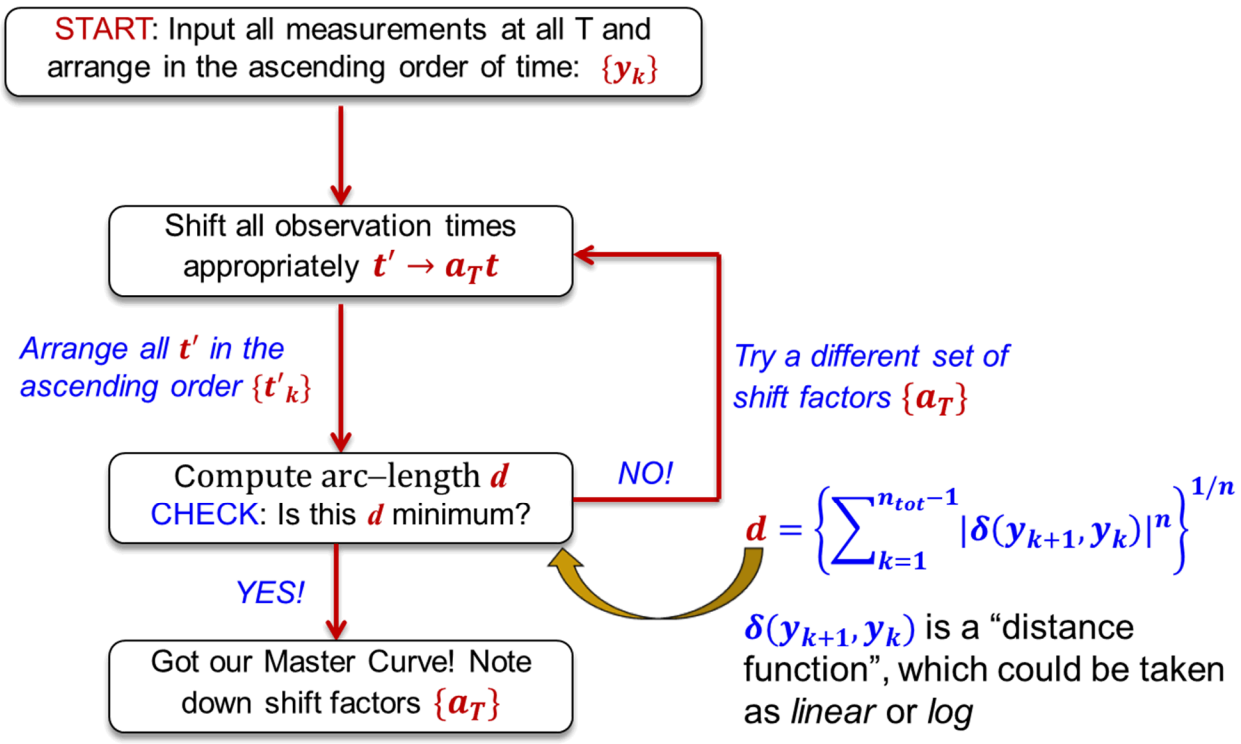

Figure A3. schematic description of the minimum arc-length method to perform automated TTS procedure for accurate aging predictions. More details are available in ref. [6].

APPENDIX III: Fitting parameters for various materials

Table 1. Parameters for the evolution of compression set ($S(t)$) of a few legacy foams. Also shown are the activation barriers (ΔE) from the slope of $\ln(shift\ factor)$ vs. $1/T$ plots

Foam	$\ln(\tau)$	m	$n^{\S}$	ΔE (kJ/mol)
M97*	3.92	0.704	2.59	66.1
M9763 (LLNL)	5.69	0.423	50	82.8
S5455	5.48	0.509	50	**
S5370	7.14	0.472	50	97.1
SE1700 (AM FCT)	12.24	0.261	50	**

§For $n = 50$ or larger, $S(t) = 1 - \exp\{-(t/\tau)^m\}$

** Did not follow Arrhenius behavior

Table 2. Parameters for the evolution of load retention ($R(t)$) of a few legacy foams, along with activation barriers (ΔE) from TTS shifts.

Foam	$\ln(\tau)$	m	$n^{\$}$	ΔE (kJ/mol)
M97*	8.329	0.350	50	93.1
M9763 (KCP)	9.840	0.247	50	67.5
M9760 (KCP)	11.182	0.164	50	75.9
SE1700 (AM FCT)	13.80	0.157	0.329	220.1

$^{\$}$For $n = 50$ or larger, $R(t) = \exp\{-(t/\tau)^m\}$

In many cases, we see that n is large (a value of larger than 50 does not make any difference), in which case: $\left\{1 + \frac{1}{n}\left(\frac{t}{\tau}\right)^m\right\}^{-n} = \exp\{-(t/\tau)^m\}$, which is a simpler, two-parameter function. However, the three-parameter form is a more generalized function that describes the $S(t)$ and $R(t)$ behavior for all Foams studied so far, including all legacy and AM foams.

APPENDIX IV: TTS-shifted data for various materials

Compression Set:

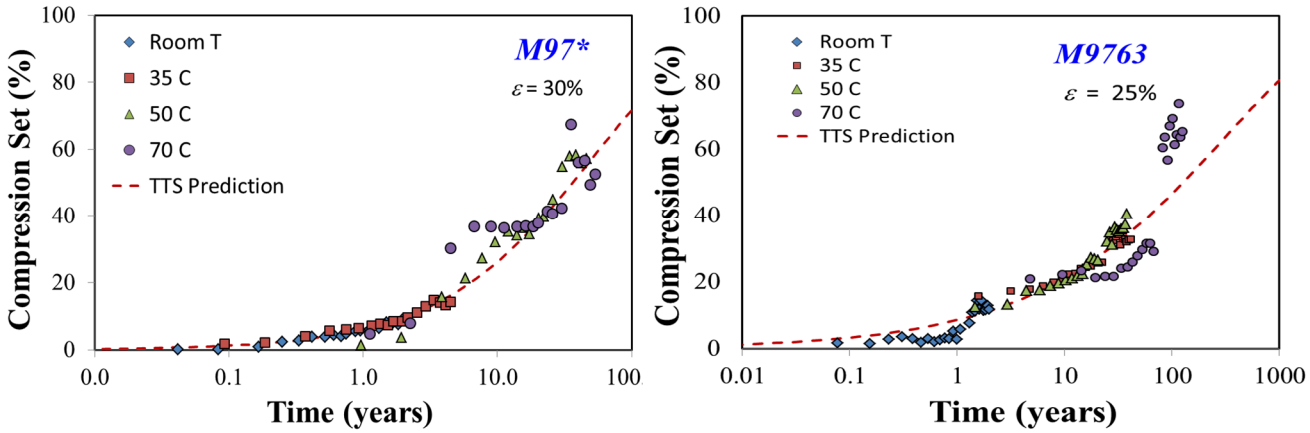

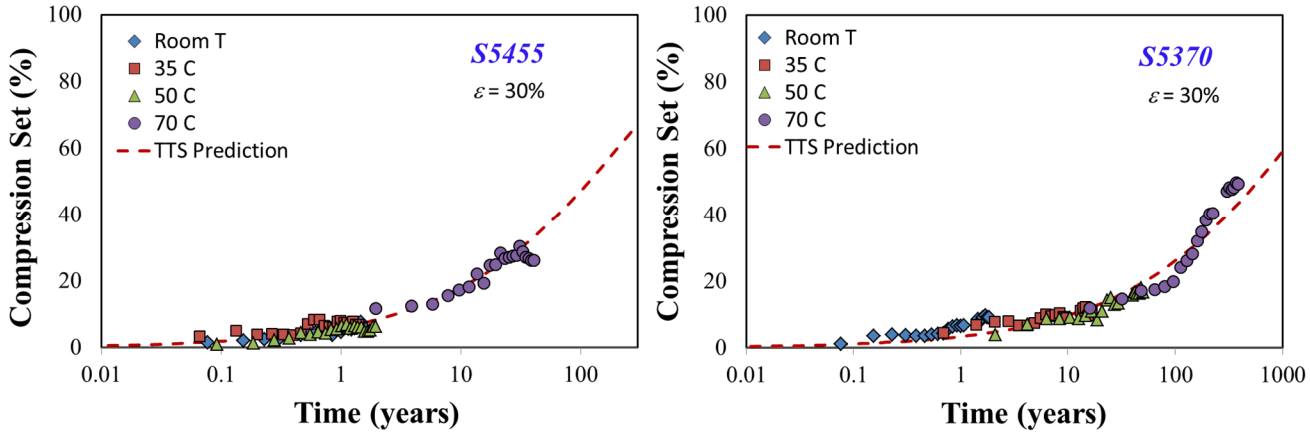

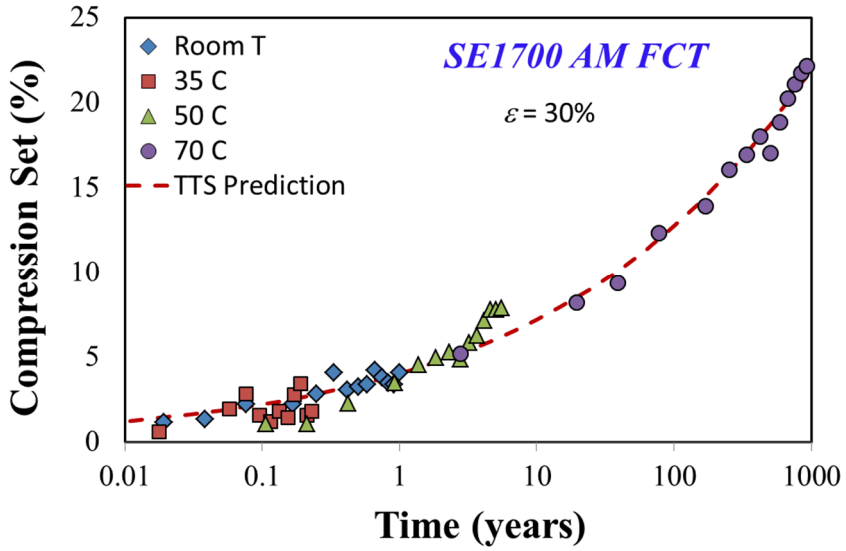

Load retention:

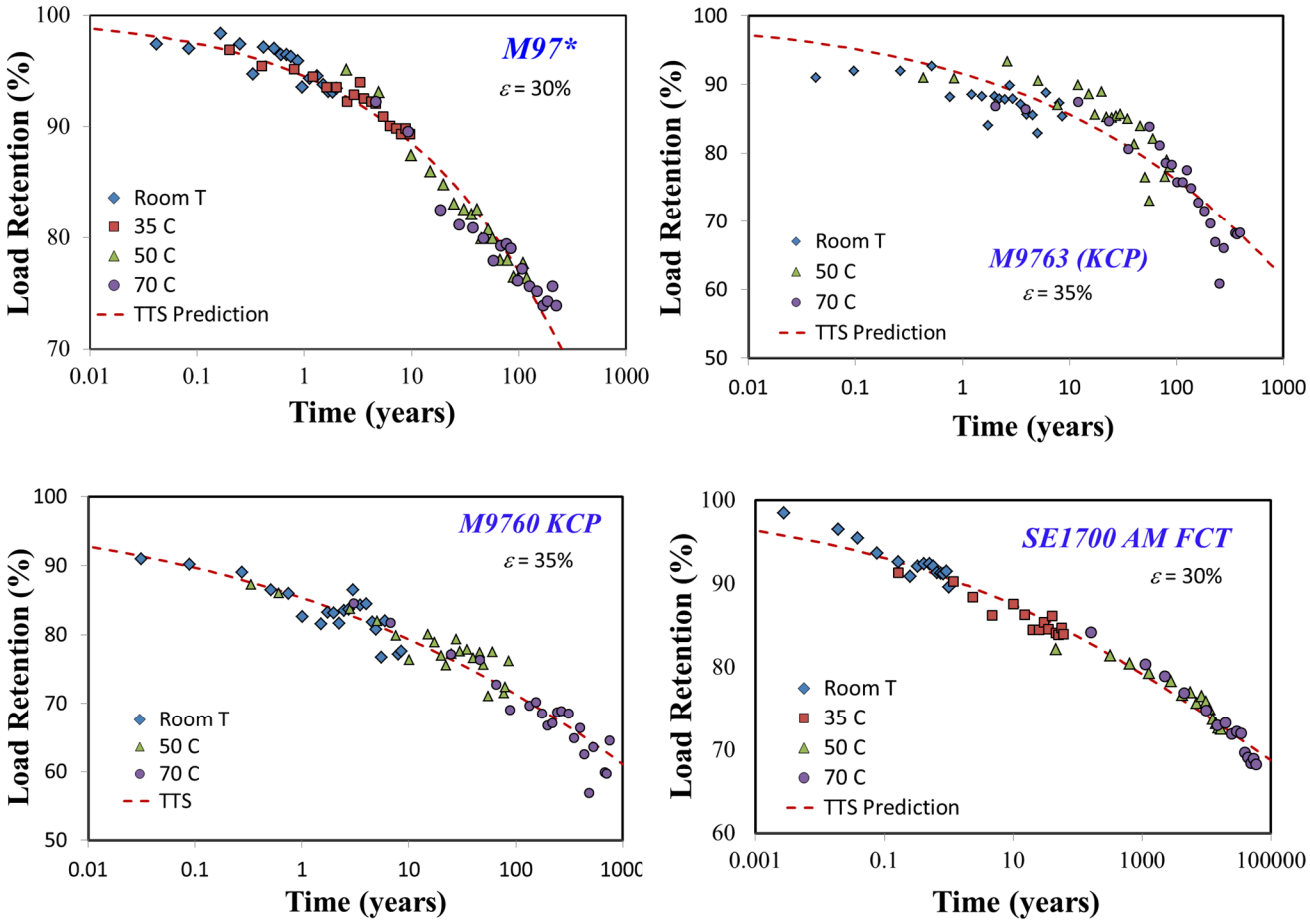

Acknowledgement. We would like to sincerely thank Dr. Jim Schneider of National Security Campus, MO (formerly Kansas City Plant) for giving us access to the results of their load retention study on the stochastic foam material. The authors would also like to gratefully acknowledge Dr Jessica Maisano and the University of Texas High-Resolution X-ray CT Facility for performing all CT scanning of the materials presented here. This work was performed under the auspices of the US Department of Energy by Lawrence Livermore National Laboratory under Contract DE-AC52-07NA27344.

References:

1. Ferry, J. D., *Viscoelastic properties of polymers*, John Wiley and Sons, New York (1980).
2. Aklonis, J. J. & MacKnight, W. J., *Introduction to Polymer Viscoelasticity*, Wiley-Interscience, New York (1983).
3. J. Zhao J, W. G. Knauss, and G. Ravichandran, *Mech. Time-Depend. Mater.* **11**, 289 (2007).
4. W. G. Knauss, *Mech. Time-Depend. Mater.* **12**, 179 (2008).
5. J-E. Bae, K. S. Cho, K. H. Seo, and D-G. Kang, *Korea-Aust. Rheol. J.* **23**, 81-87 (2011).
6. A. Maiti, , *Rheo. Acta.*, 55, 83 (2016).
7. L. J. Gibson and M. F. Ashby, *Cellular Solids, Structure and Properties*, Cambridge University Press, UK (1999).
8. S. Youssef, E. Maire, and R. Gaertner. *Acta Mater.* 53, 719 (2005).
9. E. Zywicz and J. I. Lin. *DYNA3D: A Nonlinear, Explicit, Three-Dimensional Finite Element Code for Solid and Structural Mechanics: Version 13.1*, Lawrence Livermore National Laboratory, (2013).
10. L. R. G. Treloar, *The Physics of Rubber Elasticity*, Clarendon Press, Oxford, UK (1975).
11. Simpleware ScanIP : 3D Image visualization and processing software, website: http://www.simpleware.com/software/scanip/, Date of access 15/12/2015.
12. M. A. Puso, *NIKE3D: A Nonlinear, Implicit, Three-Dimensional Finite Element Code for Solid and Structural Mechanics*, Lawrence Livermore National Laboratory (2012).
13. M. A. Puso and S. Govindjee, A phenomenological constitutive model for rigid polymeric foam. *Mech. Plast. Plast. Compos.* ASME MD **68**, 159-176 (1995).
14. N. Mills, N. *Polymer Foams Handbook*, Elsevier Science (2007).
15. A. Maiti *et al.*, *Scientific Report* **6**, 24871 (2016), http://www.nature.com/articles/srep24871.
16. R. W. Ogden, *Proc. Roy. Soc. London* **A328**, 567 (1972).
17. J. Bergstrom, *Mechanics of Solid Polymers: theory and Computational Modeling*, Elsevier (2015).
18. G. A. Holzapfel, *Nonlinear Solid Mechanics*, Wiley (2000).
19. E. Zywicz, *The Development of DYNA3D Material Model 67 - Hyperelastic Elastomeric Foam With Viscoelasticity*, LLNL-TR-666388 (2015).
20. R. S. Maxwell, and B. Balazs, *J. Chem. Phys.* **116**, 10492 (2002).
21. A. Chien, R. S. Maxwell, D. Chambers, B. Balazs, and J. LeMay, *Rad. Phys. And Chem.* **59**, 493 (2000).